A method for the direct analysis of quenched, magmatic-hydrothermal fluids recovered from high-pressure, high-temperature experiments

Austin M Gion, Fabrice Gaillard, Nicolas Freslon, Saskia Erdmann, Ida Di Carlo

Journal Pre-proof

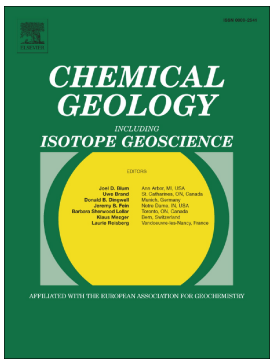

A method for the direct analysis of quenched, magmatic-hydrothermal fluids recovered from high-pressure, high-temperature experiments

Austin M. Gion, Fabrice Gaillard, Nicolas Freslon, Saskia Erdmann, Ida di Carlo

PII: S0009-2541(22)00355-2

DOI: https://doi.org/10.1016/j.chemgeo.2022.121061

Reference: CHEMGE 121061

To appear in: *Chemical Geology*

Received date: 13 June 2022

Revised date: 8 August 2022

Accepted date: 10 August 2022

Please cite this article as: A.M. Gion, F. Gaillard, N. Freslon, et al., A method for the direct analysis of quenched, magmatic-hydrothermal fluids recovered from high-pressure, high-temperature experiments, *Chemical Geology* (2022), https://doi.org/10.1016/j.chemgeo.2022.121061

A Method for the Direct Analysis of Quenched, Magmatic-Hydrothermal Fluids Recovered from High-Pressure, High-Temperature Experiments

Austin M. Gion[1,1,*] austin.gion@cnrs-orleans.fr, Fabrice Gaillard[1], Nicolas Freslon[1], Saskia Erdmann[1], and Ida Di Carlo[1]

[1]Univ. Orléans, CNRS, BRGM, ISTO, UMR 7327, F-45071 Orléans, France
[*]Corresponding author.

Abstract

A method for analyzing low-salinity fluids (up to ~ 11wt% NaCl equivalent) that have been equilibrated with felsic melts in high-pressure, high-temperature experiments is reported. Experiments were performed at a pressure of 200 MPa and 800°C in internally-heated pressure vessels, wherein magmatic fluids were quenched and recovered in a multi-step process for analyses of major (Na, K, Ca, Cl, and F) and trace (Li, Be, Mn, Cu, Zn, Rb, and Sr) elements by ion chromatography and inductively coupled plasma mass spectrometry (ICP-MS). The quenched melts were analyzed for major and trace elements by electron microprobe and laser ablation inductively coupled plasma mass spectrometry (LA-ICP-MS). Such analyses permitted the composition of the fluid to be directly measured without the need for mass balance calculations or trapping fluids within fluid inclusions while still enabling the precise determination of partition coefficients. Mass balance calculations tend to overestimate Na, K, Ca, and Be; underestimate Cu, Zn, and F; and are in agreement for Li, Mn, Rb, Sr, and Cl when compared to direct measurements. Additionally, a comparison of partition coefficients calculated from measured and mass balance derived concentrations to available literature data is consistent with mass balance calculations being less accurate than measured values. Thus, direct measurements of quenched fluids by ion chromatography and ICP-MS offer a robust method for

[1] Present Address: Univ. Orléans, CNRS, BRGM, ISTO, UMR 7327, F-45071, Orléans, France;

characterizing the composition of magmatic-hydrothermal fluids that have been equilibrated with silicate melts.

Keywords: Magmatic-hydrothermal fluids, Ion Chromatography, (LA)-ICP-MS, direct measurement; mass balance

1. Introduction

Magmatically derived fluids play a crucial role in linking the Earth's interior and surface. These fluids are responsible for the transportation of volatiles (H_2O, F, Cl, S, CO_2) and some trace elements (e.g. Li, Cu, Mo, etc.) from Earth's mantle and lower crust to its upper crust and surface. In order to understand these mass transfers, it is imperative to determine the behavior of volatiles and metals in magmatic-hydrothermal systems. A primary method of constraining this behavior is through laboratory experiments such as the previous studies on fluid/melt partitioning for granitic systems given in Table 1.

The first challenge experimental studies face is independently determining what the compositions of fluids and melts are when they are both present and in equilibrium. Generally, fluid compositions are either constrained by a mass balance calculation or directly measured by the characterization of either synthetic fluid inclusions or quenched fluids (e.g. Webster et al., 1989; Zajacz et al., 2008; Iveson et al., 2019). Additionally, in-situ techniques such as hydrothermal diamond-anvil cells combined with synchrotron analyses (e.g. Borchert et al., 2009, 2010) have been used; however, these types of studies are limited in number and discussion of the technique will not be included here. Both the mass balance and direct measurement techniques have their own strengths, benefits, and uncertainties. Mass balance calculations offer the promise of determining the concentration of a larger number of elements in

the fluid by observing the changes in the composition of the silicate melt; however, there is often uncertainty in the masses of the phases present, particularly in multi-phase systems involving a melt, a fluid, and crystals; the composition of those phases; or if there is any mass exchange with or across noble metal capsules. This can result in over- or underestimation of true fluid compositions and wider ranges of reported partition coefficients. For example, the fluid-melt partition coefficients for beryllium, and a variety of other elements, reported by experimental studies utilizing a mass balance approach have a broader range of values compared to natural fluid inclusion studies (Webster et al., 1989; Zajacz et al., 2009). Additionally, elements like copper and other chalcophile metals can easily alloy with noble metals making mass balance calculations complicated (Zajacz et al., 2011). In some cases, the noble metal capsule may also act as a source of contamination and may contain several to tens of ppm of metals such as Cu, Pd, and Ag and given the large mass ratio of capsule to starting materials these trace metals may be present in sufficient concentrations to disrupt mass balance calculations. Thus, it is unclear if a mass balance technique can reliably calculate the concentration of all elements (e.g. Iveson et al., 2019).

Fluid inclusion studies have become increasingly popular and have benefited from the advancement in experimental techniques (e.g. Sterner and Bodnar, 1984; Li and Audétat, 2009). Determining the trace element concentrations of fluid inclusions requires pre-existing knowledge of the concentration of some element or element ratio in the fluid. The known element is usually sodium, in the form of $NaCl_{equiv}$ which is determined by microthermometry. The sodium concentration is calculated by correcting the measured $NaCl_{equiv}$ for the presence of other salts by using either a mass or charge balance approach and then that concentration is used as the internal standard. However, in the case of a mass balance based reduction of data (Heinrich et al., 2003),

there is a lack of data available for systems that are dominated by salts other than NaCl, which can result in the overestimation of trace elements (Allan et al., 2005; Pettke et al., 2012). A charge balance based reduction of data (Allan et al., 2005) may improve the calculations, but still requires accurate determination of chlorine from $NaCl_{equiv}$. Accurate determination of $NaCl_{equiv}$ can be hampered by the presence of other elements, such as boron, lithium, and fluorine (Sirbescu et al., 2013); the presence of clathrates in CO_2-bearing fluids (Fall et al., 2011); the presence of multivalent salts (i.e. $CaCl_2$); and elements that may form chlorides, hydroxides, sulfides/sulfate, etc. (i.e. iron). Additionally, depending on the host of the fluid inclusions, it is necessary to separate the signal of the host from the fluid inclusion during analyses by laser ablation inductively coupled mass spectrometry. For systems where this host is quartz the separation of signals may be simple, but for more complex hosts such as sulfides or oxides this process can be more challenging. Thus, there may be greater uncertainty in fluid inclusion studies if the above issues are not fully considered. Furthermore, fluid inclusion studies often require dedicated instruments (Pettke, 2008; Pettke et al., 2012), which may make this technique less approachable to some researchers.

Given the uncertainties in mass balance calculations and the potential problems related to microthermometry and data reduction in fluid inclusion studies, it is necessary to develop alternative techniques to complement these methods and increase the accuracy of fluid measurements. One alternative method is the direct measurement of quenched fluids (e.g. Iveson et al., 2019). Here, we present a method that goes beyond current quench fluid measurements in order to measure the major (both cations and anions) and trace element concentrations of fluids that have been equilibrated with silicate melts in high-pressure, high-temperature experiments.

2. Experimental Methods

2.1. Experimental Setup

Experiments were performed to test the extent to which a fluid equilibrated with a felsic melt can be quenched, recovered, and analyzed. The starting material for the experiments reported here include powdered Bishop Tuff rhyolite (e.g. Hildreth, 1979), courtesy of Bruno Scaillet; a quartz chip (1.5 x 1.5 x 5 mm rectangle) to buffer the activity of SiO_2; and an aqueous sodium-potassium chloride solution with variable composition. The compositions of the starting materials are given in Table 2 and the ratio of Bishop Tuff to starting fluid was between 0.5 and 1 (Table 3). At the pressure (200 MPa) and temperature (800°C) of the experiments the aqueous chloride solution is a supercritical fluid with up to ~11 wt % NaCl equivalent. In one experiment, fluorine was added as a mixture of NaF, KF, and AlF_3 in a ratio of 1:1:2 in order to maintain the ASI (aluminum saturation index defined as $Al_2O_3/(Na_2O + K_2O + CaO)$ on a molar basis) of the Bishop Tuff (ASI = ~1). Amorphous SiO_2 was also added to the experiment containing the fluoride mixture in order to compensate for the additional alkalis. Starting materials were loaded into gold capsules (5 mm outer diameter, 20 mm length, 0.2 mm wall thickness) and the quartz chips were contained within an open smaller, inner gold capsule (3 mm outer diameter, 7 mm length, 0.2 mm wall thickness). Prior to loading the starting materials, the capsules were cleaned in a bath of boiling HCl followed by a bath of boiling demineralized water to remove any contamination on the capsule surface. Capsules were then annealed with an oxy-methane flame. Once annealed, capsules were then tri-crimped on one end and welded shut using a Puk spot welder. The starting materials were then loaded into the capsules and they were sealed by tri-crimping and welding the open end. Capsules were then weighed and placed in a drying oven at 120°C overnight to check for leaks. Capsules exhibiting weight loss (>1 mg) were discarded. The weights of the starting materials are given in Table 3.

Experiments were conducted in vertically oriented internally-heated pressure vessels (IHPV) at the Institut des Sciences de la Terre d'Orléans (ISTO), France (CNRS, BRGM, Université d'Orléans) at a temperature of 800°C and a pressure of 200 MPa for a duration of ~1 week. Vessels were pressurized with a mixture of pure argon and Ar-H_2 (2 vol% hydrogen). The vessel was first pressurized with 30 MPa of the Ar-H_2 mixture, to maintain a consistent oxygen fugacity during the experiment (~QFM; Table 3), followed by 130-140 MPa of pure argon. The final pressure was achieved upon heating. The oxygen fugacity of the experiments was measured after quench by using CoPd sensors (Taylor et al., 1992), which were placed in a separate capsule next to the experimental charges. These separate capsules contained cobalt and palladium powder, water, and the interiors were lined zirconia powder to limit chemical interaction with the capsule wall. Upon completion of the experiment the sensor charges were inspected to confirm the presences of a CoPd alloy, CoO, and water. Upon completion of each experiment, the capsules were quenched by one of two methods: a "slow" and "rapid" quench. The two quench methods were used to evaluate if the quench method and speed have a significant effect on the run products, such as back-reaction of the aqueous solution with the glass or greater amounts of precipitation from the fluid phase. Method one, used in three experiments, was a "slow" quench and was achieved by turning off the power to the IHPV and allowing the vessel to cool via water circulating continuously around the vessel. Method two was a "rapid" drop-quench, used in one experiment, which was performed in a two-step manner. Initially the experiment was quenched by turning off the power to the vessel. The capsule was then removed and reloaded into the vessel, re-pressurized, and re-heated to run conditions, and held for one additional hour. After one hour the capsule was drop quenched. Drop quench was achieved by placing the capsule inside an alumina basket that is suspended by a thin platinum wire. When a

current is passed across the wire it heats and breaks. The alumina basket then falls to the cold end of the vessel and the capsule is quenched. The second method required two steps because the wire holding the alumina basket generally breaks after ~24 hours due to oxidation. Quenching by using method one cools the glass to below the glass transition temperature within a few minutes and for method two the glass cools to below the glass transition temperature within a few seconds.

2.2. Recovery of Run Products

Recovery of the quenched aqueous solutions and any quench precipitates, which are analogous to the supercritical fluid, was achieved through a multistep processes after the method of Iveson et al. (2019). The recovery process is designed to dissolve any fluid or quench products in multiple fluid aliquots of large enough volume that they can be analyzed and the concentration of major and trace elements in those aliquots can be quantified. The recovery process is detailed in Iveson et al. (2019) and a general description of the steps taken in this study are presented below and outlined in Figure 1. Post-experiment capsules were removed from the vessels and cleaned in an acetone bath in a sonic wash to remove contamination on the outside of the capsule. After cleaning, capsules were weighed to assess any weight loss that occurred during the experiment. Capsules exhibiting negligible weight loss or gain (less than ± 0.5 mg) were deemed successful. Cleaned capsules were then placed in a vial with a weighed amount (5 ml by volume) of demineralized water and punctured while submerged. The opening of the capsules was confirmed by bubbles exiting the capsule. The vial was then sealed and agitated. Capsules remained submerged for at least one week to ensure the quench fluid completely mixed with the demineralized water and any water-soluble quench products were re-dissolved. The capsules were then removed from the water and dried at 120°C overnight and

then weighed to determine the mass of the quench fluid recovered by difference. The water in which the capsules were soaked was then sampled for analysis by ion chromatography by pipetting 50-100 µl into a glass vial. Once dried, capsules were opened using a straight edge razor, reweighed, and placed in a weighed amount (10 mL by volume) of 5 M HCl in a Teflon beaker at 60°C for 20 minutes to dissolve water insoluble precipitates. The capsules were then removed from the acid and dried overnight. Once dried, the capsules were weighed to determine the mass of precipitates dissolved. The capsules were inspected after the acid-soaking step to determine if any precipitates remained. In the case where salts did not fully dissolve or were re-precipitated on the capsule walls, the capsules were re-soaked in acid. Precipitates that were insoluble in the HCl were not observed. Note that in the experiments performed here, very few precipitates were observed often resulting in no mass change after the acid-soaking step. The soak solution was then added to the HCl solution. The vial containing the soak solution was rinsed out with 1 mL of 5 M HCl twice to fully recover the solution. The mixture of the soak and HCl solution was then dried overnight on a hot plate at ~70°C. The dried down precipitates were then re-dissolved in a weighed amount (5 ml by volume) of 0.28M nitric acid to be analyzed by solution ICP-MS (inductively coupled plasma mass spectrometry). This process produced solutions that were diluted by 100 to 300 times. The quartz chips were also recovered and weighed in order to accurately determine the mass of the melt by difference for the mass balance calculation. This was done because the glass tended to fracture and recovery of all pieces was not possible and thus could not be accurately weighed. Once the masses of the quartz and run product fluid were known, and assuming the weight of the gold capsule does not change significantly, the mass of the glass can be calculated by difference. The run product glasses, analogous to the melts, were removed from the capsules, mounted in epoxy, and polished for

electron microprobe and laser ablation ICP-MS analysis. The final masses of the melt and fluid phases are given in Table 3 and examples of backscatter electron images of samples are given in the supplementary information.

3. Analytical Methods

3.1. Ion Chromatography

The concentrations of major cations and anions in the quench fluids were measured by ion chromatography (IC) and were carried out by using a ThermoFisher Dionex ICS-6000 instrument. Samples of the soak solutions were diluted by a known factor of 10 with 0.01 M nitric acid for cation analyses (Na^+, K^+, Ca^{2+}, Mg^{2+}) and ultrapure water (18.2 MΩ cm resistivity) for anion analyses (F^- and Cl^-). Cations and anions were analyzed in isocratic modes by using a Dionex IonPac CG12AA column (20 mmol methanesulfonic acid eluent) and Dionex IonPac AS11-HC-4µm column (30 mM potassium hydroxide eluent), respectively. Calibration of the instrument was performed by using 10 solutions of different concentrations diluted from two commercial multi-element solutions (Merck 1.09032.0001 and Merck1.09036.0001for anions and cations, respectively) between 2 and 200 times. Analytical precision of the instrument was estimated by repeated analyses of an in-house standard every 5-10 samples. The reproducibility and accuracy of these repeated analyses is between 5 and 10% (RSD) for all cations and anions presented. In the case of one sample, an aliquot of the final nitric acid solution intended for ICP-MS analyses was sampled, dried down in a PFA beaker on a hotplate at 130°C, and recovered with 0.01 M nitric acid solution for cation analysis. This optional step was useful for highly diluted samples in order to increase the signal-to-noise ratio and improving the quantification of the concentration of sodium and potassium. Note, analysis by ion chromatography permits more

accurate analyses of major cations and anions, which varies from Iveson et al. (2019) who only analyzed the soak fluid for chlorine by chloridometery.

3.2. Solution ICP-MS

The concentration of trace elements in the quenched fluids (mixed solutions) were analyzed by inductively coupled plasma mass spectrometry (ICP-MS) by using a ThermoFisher Element-XR ICP-MS in low and medium resolutions. Samples were introduced to a hot plasma (1200V) with a 100 μl min^{-1} nebulizer and a quartz cyclonic chamber. All samples, blanks, calibration and standard solutions were prepared with 0.28 M nitric acid and were spiked with internal standards (2 ppb In-Re) in order to monitor and correct for instrumental drift. The unknown samples were diluted by an additional 10 times, producing solutions with an overall dilution factor between 1,000 and 10,000. Calibration curves were generated by analyzing three different multi-element solutions diluted to produce seven to ten solutions of different concentrations per multi-element solution. The first standard solution of trace elements included Li, Be, Sc, V, Cr, Mn, Fe, Co, Ni, Cu, Zn, Ga, Rb, Sr, Y, Zr, Nb, Cd, Ba, Hf, Pb, Th, U and was diluted to concentrations between 0.01 and 10 ppm. The second standard solution included rare-earth elements and was diluted to between 0.001 to 1 ppm. The third standard solution for major elements included Al, Si, Ca, Ti, Mn, Fe diluted between 0.01 to 100 ppm. The analytical precision was estimated by repeated analyses of HCl-HF dissolved USGS certified reference material (BIR-1, BHVO-2, and BCR-2) diluted by a factor of between 5,000 and 10,000. The external reproducibility is better than 5% (RSD) for all measurable elements and an accuracy of between 5 and 10% (RSD) for all elements, excluding silicon which is lost during preparation of the standard (i.e. partial evaporation as SiF_4).

3.3. *Electron Probe Microanalysis*

Glass run products were analyzed by using a Cameca SX-Five electron probe microanalyzer (EPMA). Wavelength dispersive spectroscopy (WDS) was used to analyze Si, P, Ti, Al, Fe, Mg, Mn, Ca, Na, K, Cl, and F. Counting times for all elements except fluorine were 10 seconds on peak and 5 seconds on background; for fluorine the counting time was increased to 30 seconds on peak and 15 seconds on background to lower the detection limit. The conditions of the electron beam were an accelerating voltage of 15 kV, a current of 5 nA, and a beam diameter of 20 microns to limit the diffusion of sodium and potassium in glass away from the electron beam (Morgan and London, 1996). The standards were albite, topaz, andradite, apatite, orthoclase, vanadinite, $MnTiO_3$, Fe_2O_3, and MgO. In addition to the run products, four rhyolite glasses with a known composition were analyzed as unknowns. These rhyolite glasses are hydrated equivalents of the dry synthetic glass reported in Table 1 of Scaillet and Evans (1999) that were doped with variable amounts of water. The water concentration of these glasses had previously been measured by Karl Fischer titration and determined to be anhydrous or have 2.42, 4.24, and 6.38 wt% water, respectively (Scaillet and Evans, 1999). Analyses of these glasses during the analytical sessions allowed the water content of the run product glasses and loss of sodium and potassium due to diffusion away from the electron beam to be estimated. The concentration of sodium in the analyzed rhyolite glasses was within uncertainty of the rhyolite glass from Scaillet and Evans (1999) for all water contents, excluding one analysis of the glass with 2.42 wt% water. For potassium, the concentrations of the analyzed glass were slightly greater (up to 0.2 wt%) than the reported values in Scaillet and Evans (1999). See supplementary files for analyses of rhyolite standards. These results are consistent with no sodium or potassium loss during EPMA analyses. Energy dispersive spectroscopy (EDS) semi-quantitative line scans were also performed on select glasses from core-to-rim in order to identify

if an ion exchange reaction between the glass and fluid occurred during quench. These line scans were performed by using a ZEISS Merlin Compact SEM equipped with a Bruker EDS detector. All EPMA and SEM analyses were performed at ISTO-CNRS-BRGM, Orléans, France.

3.4. LA-ICP-MS

The concentrations of trace elements in run product glasses were measured by laser ablation inductively coupled mass spectrometry (LA-ICPMS). All analyses were performed by using a RESOlution-SE Ar-F excimer laser (193 nm) with a S155 Laurin Technic sample cell coupled to a triple quadrupole Agilent 8900 mass spectrometer at ISTO-CNRS-BRGM, Orléans, France. The operating conditions of the laser were a spot size of 50 microns, a fluence of ~4 J/cm^2 and a repetition rate of 10 Hz. Helium (~400 ml/min) and argon (~0.92 l/min) were added to the cell and argon (0.9 l/min) was introduced into the torch as auxiliary gas. The plasma was sustained at an argon flow rate of 15 l/min and an RF power of 1480 W. The reference material NIST 612 was used for tuning to minimize fractionation (U/Th of ~1), oxide production of (ThO/Th ~0.14 to 0.26), and doubly-charged ions (Ca^{2+}/Ca^{+} ~0.28 to 0.38). The isotopes analyzed as part of this study are Li^7, Be^9, Si^{28}, Mn^{55}, Cu^{63}, Zn^{66}, Rb^{85}, and Sr^{88} and were part of a suite of 46 total isotopes analyzed. Analytical dwell time was 10 ms per isotope; the total integration time per sweep was 0.5180 seconds. For each time-resolved analysis, the background was measured for 30 seconds, followed by 50 seconds of ablated sample analysis, followed by another 10 seconds of background analysis and 15 seconds of washout. Sample analyses (15 analyses) were bracketed by analyses of reference materials. The external standard was NIST610. The reference materials NIST612, BCR-2G, and BHVO-2G were also analyzed as unknowns to monitor accuracy and precision. For NIST612, the vast majority of elements were

within uncertainty of the accepted values with a bias of between -4 and 9% relative to the accepted values. For BCR-2G and BHVO-2G the bias was greater due to poor matrix matching. The samples in this study are high-silica rhyolites and thus the matrix is similar to that of the NIST standards. Data reduction was performed by using the program SILLS (Guillong et al., 2008) and the internal standard for data reduction was SiO_2. Compositions used for NIST610, NIST612, BCR-2G, and BHVO-2G are those provided on the GeoRem website (May 2022) and Pearce et al. (1997).

3.5. Mass Balance

A mass balance calculation was performed in addition to a complete recovery and analysis of the quench fluid. The masses of the fluid, melt and starting materials, as well as the composition of the starting materials and quenched melt is required in order to calculate the compositions of the fluid phase by mass balance. The mass of the fluid is known by weighing the capsules before and after each step in the recovery process and calculating the mass by difference. The mass of the melt is calculated by difference after recovering and weighing the quartz chip and assuming the gold capsules were inert and no mass exchange across the outer capsule wall occurred. The compositions of the initial glass and quenched melt were obtained by EPMA and LA-ICP-MS as described above. Once the mass of the melt and fluid, as well as the composition of the melt is known, the composition of the final fluid phase is then calculated using the following equation:

$$C_i^{Fluid} = \frac{[(M^{o,Glass} * C_i^{o,Glass}) + (M^{o,Fluid} * C_i^{o,Fluid}) + (M^{o,F\ Mix} * C_i^{o,F\ Mix})] - (M^{Melt} * C_i^{Melt})}{M^{Fluid}}$$

where, C_i^{Fluid} is the concentration of element *i* in the fluid; $M^{o,Glass}$ is the mass of the starting glass; $C_i^{o,Glass}$ is the concentration of element *i* in the starting glass; $M^{o,Fluid}$ is the mass of the

starting fluid; $C_i^{o,Fluid}$ is the concentration of element *i* in the starting fluid; $M^{o,F\ Mix}$ is the mass of the fluorine mixture; $C_i^{o,F\ Mix}$ is the concentration of element *i* in the starting fluorine mixture; M^{Melt} is the mass of the melt at pressure and temperature; C_i^{Melt} is the concentration of element *i* in the melt at pressure and temperature; and M^{Fluid} is the mass of the fluid. The masses and concentrations of element *i* in the starting fluid and fluorine mix can be excluded for those elements that are not present. These terms only need to be included for elements such as Na, K, Cl, F, and Al.

4. Results and Discussion

4.1. General Observations of Run Products

All run products were comparable in regard to the macroscopic properties of the quench fluids and glasses. Upon piercing of the capsules while submerged in distilled water, gas bubbles were released from the capsules. There were no observable color changes or cloudiness introduced by mixing the quench fluids with the distilled water. Additionally, very few quench precipitates were observed after the capsules were removed from the soak solution and dried. In all experiments, the mass of the quench precipitates measured by difference during the recovery process was ≤1 mg. The run product glasses for all fluorine-free experiments yielded a translucent glass with numerous bubbles and no observable crystalline phases. The bubbles are part of the supercritical fluid phase; however, because they are trapped in the glass and their volume and exact number are unknown they are not recovered nor weighed. Thus, their mass is included in the mass of the melt. This introduces uncertainty in the mass balance calculation, but given the mass of the quenched fluid recovered is approximately that of the starting fluid this uncertainty is likely minor in the present study. However, in some cases particularly if a large number of bubbles form, the uncertainty may be higher. For example, if a melt (density of 2.4

g/cm^3) has a bubble number density of 10^6 bubbles/cm^3 with an average diameter of 30 microns that are ~60% filled with a ~2 *m* $NaCl_{equiv}$ fluid at room pressure and temperature (all values estimated from Larsen and Gardner (2000) and Klyukin et al. (2019)) then the uncertainty in the mass of the melt is ~5%. Note, these bubbles do not affect the measured values as only the mass of the recovered fluid is needed for the ICP-MS and ion chromatography analyses. In the fluorine-bearing experiment, the crystalline phases present included quartz and alkali feldspar, along with clusters of biotite and fluorite crystals. The individual crystals in the fluorine-bearing experiment were generally less than 5μm in size. Quartz is the most abundant crystalline phase (~1-2 modal percent) found in zones dispersed throughout the glass along with lesser amounts of plagioclase. The clusters of biotite and fluorite are dispersed throughout the glass and are estimated to be less than 1 modal percent.

4.2. Compositions of Run Products

The major element and select trace element concentrations of the run product glasses are reported in Table 4. The run product glasses are hydrated equivalents of the starting material, with minor changes in the Na/K ratio and trace element compositions due to equilibration with the fluid phase. The measured compositions of the quench fluids are reported in Table 4 and the compositions calculated by mass balance are reported in Table 5. The quench fluids are aqueous chloride solutions with minor fluorine. In several of the experiments, fluorine was not added but minor amounts of fluorine were measured and this fluorine was sourced from the starting glass. The Bishop Tuff has up to a few hundred ppm fluorine (Mahood and Hildreth, 1983) but this concentration is below detection (~1000 ppm) of the EPMA analyses for the glasses used here. The composition of the quench fluid is a function of the starting fluid composition and the majority of the trace elements vary as a function of the chlorine concentrations such that Na, K,

Ca, Li, Mn, Rb, and Sr increase with increasing chlorine content, whereas Be, Cu, Zn have no change or exhibit a decrease with increasing chlorine content (Figure 2).

Partition coefficients for both the mass balance calculation and the measured values were calculated by

$$D_i^{Fluid/Melt} = \frac{C_i^{Fluid}}{C_i^{Melt}}$$

where $D_i^{Fluid/Melt}$ is the partition coefficient for element *i* between the fluid and the melt, C_i^{Fluid} is the concentration of element *i* in the fluid, and C_i^{Melt} is the concentration of element *i* in the melt. Partition coefficients derived from mass balance calculations and those that are derived from measurements are given in Table 6.

4.3. "Slow" vs Drop Quench

The quenching speed (a few minutes for the slow quench and a few seconds for rapid quench) of the experiment appears to have little to no effect on the results of the experiments. Neither type of experiments produced large amounts of quench precipitates. Additionally, the absolute concentrations and partition coefficients for all elements in the glass and fluid are consistent between the drop quench experiment and the "slow" quench experiments and no back reactions upon quench have been observed. Previously, Shinohara et al. (1989) reported that an ion exchange of sodium and potassium between the glass and fluid occurred upon quench, changing the ratio of sodium to potassium in the fluid. Shinohara et al. (1989) observed that in a profile of the glass from rim-to-core the sodium to potassium ratio varied and stabilized after ~100 microns away from the rim, which was interpreted as support for an ion exchange reaction during quench. The effect of an ion exchange in the experiments reported here was examined by performing EDS line scans from rim-to-core of both drop and "slow" quench glasses. Each line scan comprises 100 points each spaced a few microns apart with a total analysis time of 72

seconds per line. For each point, an EDS spectrum was obtained and quantified (semi-quantitative, standardless analysis) in order to determine the sodium/potassium ratio. Neither the drop quench nor "slow" quench experiments exhibit any systematic changes in Na/K ratios within 300 microns from the rim of the glass (Figure 3) and therefore an ion exchange or other back-reactions that may occur upon quench can be excluded for the experimental design reported here.

4.4. Mass Balance vs. Measurements

A comparison of the mass balance and measured compositions of the quench fluid for Na, K, Rb, Cu, and Cl is given in Figure 4. The concentrations of sodium, potassium, and calcium, as well as beryllium, calculated by mass balance are systematically higher than the concentrations measured by ion chromatography or solution ICP-MS. Additionally, the concentrations of fluorine (even excluding the fluorine-bearing experiment), copper, and zinc determined by the mass balance calculation are less than the measured concentrations. For lithium, rubidium, and strontium, manganese, and chlorine, the mass balance and measured concentrations are in agreement, although for lithium the agreement is weaker. In some cases, the concentrations calculated by mass balance are negative, a physical impossibility, highlighting the significant underestimation for some elements.

The results of mass balance calculations for chlorine, sodium, and potassium were further scrutinized in order to determine if the mass balance or measured concentrations are more accurate. Sodium and potassium are the most abundant cations in the fluid phase and thus it is reasonable to assume that the majority of the chlorine in the fluid phase is attached to either sodium or potassium. Thus, the molal concentrations of sodium and potassium should be approximately equal to or slightly less than the molal concentration of chlorine. The sum of the

sodium and potassium concentration may be slightly lower than the chlorine concentration in order to accommodate other cations that complex with chlorine. However, the concentration of sodium and potassium should not be significantly greater than the concentration of chlorine as the amount of hydroxide, fluoride, or ionic species that form are expected to be significantly less than the chloride species (with the exception of one experiment; see below).

A comparison of the chlorine vs sodium + potassium for both the measured concentrations and the concentrations derived from the mass balance calculation are given in Figure 5. The molal concentrations of sodium and potassium for the mass balance calculations are consistently higher than the molal concentrations of chlorine and in some cases is up to 0.5 molal higher than the chlorine. The measured molal concentrations of sodium and potassium are in agreement with or slightly lower than the concentration of chlorine, with the exception of one experiment at a low chlorine concentration (BT-4-2-S4). Fluorine was added to experiment BT-4-2-S4 as NaF and KF and thus excess sodium and potassium is likely present as a fluoride or hydroxide species. The hydroxide species are more likely as the fluorine will either generate HF or be taken up by the fluorite and biotite present in the run products. Additionally, due to the solubility differences of KF and NaF (Morey and Chen, 1956), NaF may also be present as a crystalline solid in the run products. The difference in solubility may also affect the final Na/K ratio of the fluid or melt. Although there is little variation observed in the reported melt compositions, there is some variation in the fluid composition; however, there is insufficient evidence to support that NaF or KF is the root cause of this variation. Additionally, it could be hypothesized that the fluid-to-glass ratio may influence the accuracy of the mass balance calculation. At large fluid/glass ratios, a large amount of material is transferred into the fluid to reach equilibrium resulting in an easily resolvable difference between the starting and final glass

composition. However, there appears to be little to no correlation between fluid/glass ratio and the difference between measured concentrations and concentrations calculated by mass balance for the major cations. This is consistent with other factors such as contamination influencing this difference. The discrepancy between measured and mass balance calculations for sodium and potassium highlight the potential problems with mass balance calculations. In the case reported here the data are consistent with mass balance calculations overestimating the concentrations of sodium and potassium in the fluid phase and thus, the measured concentrations are more accurate than mass balance calculations.

The partition coefficients of previous studies (Table 1) were compared to the partition coefficients reported here (Table 6) in order to determine if the over- or underestimation of major and trace elements is common in data reported in literature (Figure 6). The partition coefficients used here are for comparative purposes only, as a comparison of absolute concentrations between studies and experiments bears no significance, due to the difference in bulk composition of starting materials. The mass balance and measured partition coefficients reported here are in agreement with previous studies. However, previous studies have reported similar observations regarding differences in mass balance and measured concentrations in fluid phases. For example, the potassium concentrations calculated by Schmidt et al. (2020) by mass balance were either greater than or consistent with synthetic fluid inclusions from the same experiments, suggesting overestimation of potassium partition coefficients. Thus, it is reasonable to suggest that partition coefficients calculated by mass balance for sodium, calcium, and beryllium in previous studies are, as in this study, overestimated. Conversely, other estimates such as fluorine, copper, and zinc may be underestimated when calculated by mass balance or are, at minimum, inconsistent. For fluorine, the concentration is systematically underestimated in this

study and the one partition coefficient reported is lower than in previous studies. This underestimation may be a result of a low concentration in the starting material and high detection limits of the EPMA. At present the only other study to compare mass balance calculations and measured values for fluorine is Wu and Koga (2018) who reported large uncertainty and general scatter in their mass balance calculations. For copper, most experimental studies consider the capsule to be a sink for copper (e.g. Zajacz et al., 2011) and thus overestimating the copper partition coefficient would be expected. However, in this study the partition coefficients were underestimated. The most likely source of this additional copper is the gold capsule itself. Analyses of one batch of starting gold tubing by LA-ICP-MS is consistent with the capsule having ~5 ppm of copper, but according to the manufacturer (Ögussa) the gold may contain a maximum of 50 ppm. This is equal to or greater than the copper concentration in the starting glasses. Given the ratio of the gold capsule to starting materials (~1.3 g Au to ~0.05 to 0.1 g starting material) this copper concentration is sufficient to disrupt the mass balance calculation. The partition coefficients derived from measured values (Table 6; 32 - 380) and from a mass balance (Table 6; 11 – 28.2) for copper are generally consistent with natural fluid inclusions in felsic systems with similar salinities of 1 to 3 *m* Cl (Zajacz et al., 2008 (15 - 2698; median 34)). These values are also consistent with previous experimental studies, who report partition coefficients for copper of 20 to 433 with a median of 68.5 for fluids with salinities between 1 and 3 *m* Cl and partition coefficients of 3 to 103 with a median of 8.8 for fluids with salinities of less than 1 m Cl, excluding outliers (Williams et al., 1995; Simon et al., 2006; Tattitch et al., 2015). Because the partition coefficient for copper is strongly a function of the chloride content of the fluid, the range of values from the present study should span a similar range as previous studies (~10-1000) for fluids of similar salinity. The measured values are within this expected range;

however, the values from the mass balance calculation underestimate the partition coefficient, particularly at higher salinities (>1 *m* Cl). Thus, it is clear our mass balance calculations cannot be used for copper partitioning studies. For zinc, the concentrations and partition coefficients were underestimated in this study; however, this is inconsistent with Iveson et al. (2019) who reported agreement between mass balance and measured partition coefficients. There are also a number of elements whose mass balance calculations are consistent with measured values both in this study and previously reported (e.g. Iveson et al., 2019) including lithium, rubidium, strontium, manganese, and chlorine, suggesting that, for at least these elements, mass balance calculations are accurate. It is not clear why the mass balance for these elements is accurate between studies. However, it can be hypothesized that contamination of lithium, rubidium, strontium, manganese, and chlorine is limited in laboratory settings; whereas for other metals, particularly in experimental laboratories where metal alloys are common, contamination may be more prevalent. Additionally, the concentration of these elements may not be heavily influenced by crystals/nano-crystallites found in the run products or starting materials, which may either release or sequester the metals during the experiments. Regardless, given the overestimation of major elements like sodium and potassium and the underestimation of elements like copper and zinc it is reasonable to question the accuracy of mass balance calculations.

4.5. General Reliability of Mass Balance Calculation

A reliable mass balance calculation requires that the compositions and masses of all crystalline phases and the melt are known and there is no mass transfer during the experiment or contamination during capsule preparation. However, a number of issues may arise when trying to meet these requirements. When determining the composition of hydrous glasses by EPMA, diffusion of alkalis away from the electron beam can cause lower concentrations of sodium and

potassium in the melt to be measured and result in overestimation in the fluid (Nielsen and Sigurdsson, 1981; Morgan and London, 1996). Note, in this study there is no significant diffusion of potassium and sodium away from the electron beam (see section above) and the overestimation of sodium and potassium in the fluid cannot be explained by such diffusion. Additionally, if any crystalline phases are present, determining the masses of the melt and crystalline phases becomes increasingly complex. Techniques, such as point counting, can be used to estimate mass fractions for crystalline phases. However, this technique also assumes that area fractions can be converted into volume fractions, which requires that two-dimensional slices used for counting are representative of the entire, three-dimensional sample, and these area fractions can then be converted into mass fractions (requires the densities of all phases to be known). These conversions, particularly from area to volume, can introduce large uncertainties into mass balance calculations. It may also be difficult or impossible to determine the major and trace element compositions of all the phases due to small crystal sizes. This will be particularly problematic in systems where nanocrystallites or cryptocrystalline phases are present and if these phases have a high affinity for any metals (e.g. hafnium in zircon or europium in plagioclase). For example, in experiment BT-4-2-S4 the addition of amorphous SiO_2, NaF, KF, and AlF_3 promoted the crystallization of quartz, alkali feldspar, biotite, and fluorite. All of these phases were easily seen in backscatter electron images, but were too small to determine their composition. The composition of these phases is thus unknown and volume fractions (a few modal percent) can only be estimated with image analysis, which resulted in an overestimation (up to 65%) of the amount of sodium and potassium in the fluid phase. This overestimation is likely to extend to other trace elements that partition strongly into feldspar, biotite, or fluorite. Additionally, mass balance calculations can be inaccurate if there is any contamination of the

capsule during sample preparation, such as that noted by Iveson et al. (2019) for tungsten, or mass exchange across the capsule wall. Contamination during capsule preparation or mass exchange during the experiment will have a large effect on trace elements (e.g. copper and zinc) due to the lower concentrations in the starting materials, but is unlikely to affect major elements (e.g. sodium) due to their large concentration in the starting materials. Direct measurements of the quench fluids eliminate the need to account for crystalline phases, mass exchange, or minor contamination during capsule preparation. Instead the only requirement is that the fluid can be recovered and weighed, which, as demonstrated here, is feasible. Given the unreliability of mass balance calculations, it is suggested that they only be performed out of necessity and be treated as estimates.

4.6. Implications for Future Studies

The combination of the recovery technique developed by Iveson et al. (2019) with ion chromatography and solution ICP-MS reported here allows for the complete recovery and analysis of fluids equilibrated with felsic melts. This is a significant advancement over previous mass balance studies, which primarily focus on conditions wherein the only phases to exist are the melt and fluid. This technique can be used to determine how metals partition among melts, fluids, and crystals. This is particularly useful for studying complex systems at the magmatic-hydrothermal transition. Additionally, this style of experiment is not limited to felsic systems as this technique can easily accommodate more mafic systems, such as basalts and andesites or systems exploring the transport of metals between mafic and felsic systems (e.g. Guo and Audétat, 2017). Although in the case of more mafic systems a rapid drop quench is preferable to limit the crystallization of the melt during quench, something that is more likely in less-viscous basalts or andesites compared to the rhyolitic melts used here.

The method reported here opens the door for additional studies on fluid/melt partitioning to be performed, as well as replace mass balance techniques. In particular, the novel use of ion chromatography to determine the concentrations of sodium, potassium and calcium, as well as chlorine and fluorine will facilitate future studies on mass exchange between silicate melts and aqueous fluids. Few studies have utilized ion chromatography in order to analyze synthetic magmatic fluids and typically consider only a single element. For example, Borchert et al. (2010) determined chlorine, Wu and Koga (2018) determined fluorine, Aranovich et al. (2013) briefly considered potassium, and Peiffert et al. (1994) determined carbonates. However, analyses of a large suite of cations and anions, as reported here, has not been previously considered. Ion chromatography may also be used to analyze other major cations and anions such as iron, magnesium, sulfate, phosphate, bromates, nitrates, and carbonates from a single fluid sample. Additionally, the method described here may be more approachable to some researchers than fluid inclusion studies, which may require more specialized equipment, such as dedicated LA-ICP-MS systems. This method is not intended to be a replacement for fluid inclusion studies, but as a complement to those studies. Depending on the conditions and starting materials, future studies may face additional difficulties not reported here. For example, lower temperature studies (several hundred of degrees) may benefit from the post-experimental processes and analytical technique reported here, where fluid inclusions techniques may have additional difficulties. However, the duration of the experiment will need to be longer in order to reach equilibrium. Care will also need to be taken that the solid products (non-quench related solids) formed at these temperatures, which may include a variety of hydrothermal minerals such as clays or carbonates, do not react with the acid bath and are insoluble in water. Conversely, in systems where the fluid is prone to containing large amounts of sulfur, oxide forming

components, or dissolved gasses additional recovery steps may be needed. If sulfides or oxides precipitate during quench, other acids or combinations of acid (e.g. HNO_3, oxalic acid, sulfuric etc.) may be needed to fully re-dissolve them completely (e.g. Chao and Sanzolone, 1977; Salmimies et al., 2016). However, as noted above, testing should be performed to ensure the acid does not dissolve the solid run products. Further, this technique is not presently designed to accommodate gas species that exsolve from the fluid during decompression and an additional step would be need during capsule opening to capture these gas phase.

5. Conclusions

This study demonstrates that the composition of magmatic fluids that have been equilibrated with felsic melts during high-pressure, high-temperature experiments can be reliably recovered and characterized. Characterization of such fluids is made possible by completely recovering quenched fluids by using a multistep process coupled with ion chromatography and solution ICP-MS. This recovery and combined analyses will facilitate future studies concerning the behavior of metals and volatiles in magmatic-hydrothermal systems by permitting the composition of synthetic fluids to be determined without relying on a mass balance calculation or fluid inclusions analyses. Direct measurements are more reliable and more consistent than mass balance calculations. It is thus suggested that mass balance calculations be avoided and those calculations replaced by more reliable measurements. If mass balance calculations are needed, the results should be considered as plausible ranges of concentrations and partition coefficients. Thus, direct measurements of quench fluids offer an alternative method to fluid inclusions analysis and one that is more accurate that a mass balance calculation.

Acknowledgements

Austin M. Gion and the analytical laboratories are supported by LabEx VOLTAIRE (LABX-100-01) and EquipEx PLANEX (ANR-11-EQPX-0036). We would like to thank Brian Tattitch and Alexander Iveson for their helpful reviews, which improved the quality of this work, as well as Bruno Scaillet and Michel Pichavant for their helpful discussions and advice. Patricia Benoist is also thanked for assistance in SEM analyses. Colleagues from the Expérimentation, GEOMIN, and Mesure Physique platforms, as well as the staff of IRAMAT are thanked for their support and assistance in the operation and maintenance of the laboratories at ISTO and CNRS.

Declaration of Competing Interest

The authors declare that they have no known competing financial interests or personal relationships that could have appeared to influence the work reported in this paper.

Supplementary Information

Supplementary information including individual EPMA and LA-ICP-MS analyses of run products and LA-ICP-MS analyses of external standards are available as an excel spreadsheet alongside this manuscript. Backscatter electron images of some run products are available in the supplementary information.

Supplementary data
Supplementary material 1
Supplementary material 2

References

Allan, M.M. et al., 2005. Validation of LA-ICP-MS fluid inclusion analysis with synthetic fluid inclusions. American Mineralogist, 90(11-12): 1767-1775.

Aranovich, L.Y., Newton, R.C., Manning, C.E., 2013. Brine-assisted anatexis: Experimental melting in the system haplogranite–H2O–NaCl–KCl at deep-crustal conditions. Earth and Planetary Science Letters, 374: 111-120.

Bai, T.B., Koster van Groos, A.F., 1999. The distribution of Na, K, Rb, Sr, Al, Ge, Cu, W, Mo, La, and Ce between granitic melts and coexisting aqueous fluids. Geochimica et Cosmochimica Acta, 63(7): 1117-1131.

Borchert, M., Wilke, M., Schmidt, C., Rickers, K., 2009. Partitioning and equilibration of Rb and Sr between silicate melts and aqueous fluids. Chemical Geology, 259(1): 39-47.

Borchert, M., Wilke, M., Schmidt, C., Rickers, K., 2010. Rb and Sr partitioning between haplogranitic melts and aqueous solutions. Geochimica et Cosmochimica Acta, 74(3): 1057-1076.

Borisova, A.Y. et al., 2012. Tin and associated metal and metalloid geochemistry by femtosecond LA-ICP-QMS microanalysis of pegmatite–leucogranite melt and fluid inclusions: new evidence for melt–melt–fluid immiscibility. Mineralogical Magazine, 76(1): 91-113.

Bos, A., 1990. Hydrothermal Element Distributions at High Temperatures: An Experimental Study on the Partitioning of Major and Trace Elements Between Phlogopite, Haplogranitic Melt and Vapour., Instituut voor Aardwetenschappen Rijksuniversiteit te Utrecht, 99 pp.

Candela, P.A., Holland, H.D., 1984. The partitioning of copper and molybdenum between silicate melts and aqueous fluids. Geochimica et Cosmochimica Acta, 48(2): 373-380.

Chao, T.T., Sanzolone, R.F., 1977. Chemical dissolution of sulfide minerals. Journal of Research of the U.S. Geological Survey, 5(4): 409-412.

Chevychelov, V.Y., Chevychelova, T., 1998. Partitioning of Pb, Zn, W, Mo, Cl, and major elements between aqueous fluid and melt in the systems granodiorite (granite, leucogranite)-H~ 2O-NaCl-HCl. Neues Jahrbuch fur Mineralogie Abhandlungen, 172: 101-115.

Fall, A., Tattitch, B., Bodnar, R.J., 2011. Combined microthermometric and Raman spectroscopic technique to determine the salinity of H2O–CO2–NaCl fluid inclusions based on clathrate melting. Geochimica et Cosmochimica Acta, 75(4): 951-964.

Guillong, M., Meier, D.L., Allan, M.M., Heinrich, C.A., Yardley, B.W., 2008. SILLS: A MATLAB-based program for the reduction of laser ablation ICP-MS data of homogeneous materials and inclusions. In: Sylvester, P. (Ed.), Laser Ablation ICP-MS in the Earth Sciences: Current Practices and Outstanding Issues. Mineralogical Association of Canada Short Course 40, pp. 328-333.

Guo, H., Audétat, A., 2017. Transfer of volatiles and metals from mafic to felsic magmas in composite magma chambers: An experimental study. Geochimica et Cosmochimica Acta, 198: 360-378.

Heinrich, C.A. et al., 2003. Quantitative multi-element analysis of minerals, fluid and melt inclusions by laser-ablation inductively-coupled-plasma mass-spectrometry. Geochimica et Cosmochimica Acta, 67(18): 3473-3497.

Hildreth, W., 1979. The Bishop Tuff: Evidence for the origin of compositional zonation in silicic magma chambers In: Chapin, C.E., Elston, W.E. (Eds.), Ash-Flow Tuffs. Geological Society of America Special Volumes.

Holland, H.D., 1972. Granites, Solutions, and Base Metal Deposits. Economic Geology, 67(3): 281-301.

Iveson, A.A., Webster, J.D., Rowe, M.C., Neill, O.K., 2019. Fluid-melt trace-element partitioning behaviour between evolved melts and aqueous fluids: Experimental constraints on the magmatic-hydrothermal transport of metals. Chemical Geology, 516: 18-41.

Keppler, H., Wyllie, P.J., 1991. Partitioning of Cu, Sn, Mo, W, U, and Th between melt and aqueous fluid in the systems haplogranite-H_2O–HCl and haplogranite-H_2O–HF. Contributions to Mineralogy and Petrology, 109(2): 139-150.

Klyukin, Y.I., Steele-MacInnis, M., Lecumberri-Sanchez, P., Bodnar, R.J., 2019. Fluid inclusion phase ratios, compositions and densities from ambient temperature to homogenization, based on PVTX properties of H2ONaCl. Earth-Science Reviews, 198: 102924.

Larsen, J.F., Gardner, J.E., 2000. Experimental constraints on bubble interactions in rhyolite melts: implications for vesicle size distributions. Earth and Planetary Science Letters, 180(1): 201-214.

Li, Y., Audétat, A., 2009. A method to synthesize large fluid inclusions in quartz at controlled times and under unfavorable growth conditions. American Mineralogist, 94(2-3): 367-371.

London, D., Hervig, R.L., Morgan, G.B., 1988. Melt-vapor solubilities and elemental partitioning in peraluminous granite-pegmatite systems: experimental results with Macusani glass at 200 MPa. Contributions to Mineralogy and Petrology, 99(3): 360-373.

Mahood, G., Hildreth, W., 1983. Large partition coefficients for trace elements in high-silica rhyolites. Geochimica et Cosmochimica Acta, 47(1): 11-30.

Morey, G.W., Chen, W.T., 1956. Pressure-Temperature Curves in Some Systems Containing Water and a Salt. Journal of the American Chemical Society, 78(17): 4249-4252.

Morgan, G.B., London, D., 1996. Optimizing the electron microprobe analysis of hydrous alkali aluminosilicate glasses. American Mineralogist, 81(9-10): 1176-1185.

Nielsen, C.H., Sigurdsson, H., 1981. Quantitative methods for electron microprobe analysis of sodium in natural and synthetic glasses. American Mineralogist, 66(5-6): 547-552.

Pearce, N.J.G. et al., 1997. A Compilation of New and Published Major and Trace Element Data for NIST SRM 610 and NIST SRM 612 Glass Reference Materials. Geostandards Newsletter, 21(1): 115-144.

Peiffert, C., Cuney, M., Nguyen-Trung, C., 1994. Uranium in granitic magmas: Part 1. Experimental determination of uranium solubility and fluid-melt partition coefficients in the uranium oxide-haplogranite-H2O-Na2CO3 system at 720–770°C, 2 kbar. Geochimica et Cosmochimica Acta, 58(11): 2495-2507.

Pettke, T., 2008. Analytical protocols for element concentration and isotope ratio measurements in fluid inclusions by LA-(MC)-ICP-MS. Laser Ablation ICP-MS in the Earth Sciences: Current Practices and Outstanding Issues. Mineralogical Association of Canada, Short Course Series, 40: 189-218.

Pettke, T. et al., 2012. Recent developments in element concentration and isotope ratio analysis of individual fluid inclusions by laser ablation single and multiple collector ICP-MS. Ore Geology Reviews, 44: 10-38.

Salmimies, R., Vehmaanperä, P., Häkkinen, A., 2016. Acidic dissolution of magnetite in mixtures of oxalic and sulfuric acid. Hydrometallurgy, 163: 91-98.

Scaillet, B., Evans, B.W., 1999. The 15 June 1991 Eruption of Mount Pinatubo. I. Phase Equilibria and Pre-eruption P–T–fO2–fH2O Conditions of the Dacite Magma. Journal of Petrology, 40(3): 381-411.

Schmidt, C., Romer, R.L., Wohlgemuth-Ueberwasser, C.C., Appelt, O., 2020. Partitioning of Sn and W between granitic melt and aqueous fluid. Ore Geology Reviews, 117: 103263.

Shinohara, H., Iiyama, J.T., Matsuo, S., 1989. Partition of chlorine compounds between silicate melt and hydrothermal solutions: I. Partition of NaCl-KCl. Geochimica et Cosmochimica Acta, 53(10): 2617-2630.

Simon, A.C., Pettke, T., Candela, P.A., Piccoli, P.M., Heinrich, C.A., 2006. Copper partitioning in a melt–vapor–brine–magnetite–pyrrhotite assemblage. Geochimica et Cosmochimica Acta, 70(22): 5583-5600.

Sirbescu, M.-L.C. et al., 2013. Analysis of boron in fluid inclusions by microthermometry, laser ablation ICP-MS, and Raman spectroscopy: Application to the Cryo-Genie Pegmatite, San Diego County, California, USA. Chemical Geology, 342: 138-150.

Sterner, S.M., Bodnar, R.J., 1984. Synthetic fluid inclusions in natural quartz I. Compositional types synthesized and applications to experimental geochemistry. Geochimica et Cosmochimica Acta, 48(12): 2659-2668.

Tattitch, B., Chelle-Michou, C., Blundy, J., Loucks, R.R., 2021. Chemical feedbacks during magma degassing control chlorine partitioning and metal extraction in volcanic arcs. Nature Communications, 12(1): 1774.

Tattitch, B.C., Blundy, J.D., 2017. Cu-Mo partitioning between felsic melts and saline-aqueous fluids as a function of XNaCleq, fO2, and fS2. American Mineralogist, 102(10): 1987-2006.

Tattitch, B.C., Candela, P.A., Piccoli, P.M., Bodnar, R.J., 2015. Copper partitioning between felsic melt and H_2O–CO_2 bearing saline fluids. Geochimica et Cosmochimica Acta, 148: 81-99.

Taylor, J.R., Wall, V.J., Pownceby, M.I., 1992. The calibration and application of accurate redox sensors. American Mineralogist, 77: 284-295.

Urabe, T., 1987. The effect of pressure on the partitioning ratios of lead and zinc between vapor and rhyolite melts. Economic Geology, 82(4): 1049-1052.

Webster, J.D., 1990. Partitioning of F between H_2O and CO_2 fluids and topaz rhyolite melt. Contributions to Mineralogy and Petrology, 104(4): 424-438.

Webster, J.D., 1992. Water solubility and chlorine partitioning in Cl-rich granitic systems: Effects of melt composition at 2 kbar and 800°C. Geochimica et Cosmochimica Acta, 56(2): 679-687.

Webster, J.D., Holloway, J.R., Hervig, R.L., 1989. Partitioning of lithophile trace elements between H 2 O and H 2 O + CO 2 fluids and topaz rhyolite melt. Economic Geology, 84(1): 116-134.

Williams, T.J., Candela, P.A., Piccoli, P.M., 1995. The partitioning of copper between silicate melts and two-phase aqueous fluids: An experimental investigation at 1 kbar, 800° C and 0.5 kbar, 850° C. Contributions to Mineralogy and Petrology, 121(4): 388-399.

Williams, T.J., Candela, P.A., Piccoli, P.M., 1997. Hydrogen-alkali exchange between silicate melts and two-phase aqueous mixtures: an experimental investigation. Contributions to Mineralogy and Petrology, 128(2): 114-126.

Wu, J., Koga, K.T., 2018. Direct analyses of fluorine in aqueous fluids extracted from 1-GPa experiments. Chemical Geology, 502: 44-54.

Zajacz, Z., Halter, W.E., Pettke, T., Guillong, M., 2008. Determination of fluid/melt partition coefficients by LA-ICPMS analysis of co-existing fluid and silicate melt inclusions: Controls on element partitioning. Geochimica et Cosmochimica Acta, 72(2): 2169-2197.

Zajacz, Z., Seo, J.H., Candela, P.A., Piccoli, P.M., Tossell, J.A., 2011. The solubility of copper in high-temperature magmatic vapors: A quest for the significance of various chloride and sulfide complexes. Geochimica et Cosmochimica Acta, 75(10): 2811-2827.

Table 1

Study	Experimental Methods: Fluid "Type"	Analytical Method for Fluid	Temperature (°C)	Pressure (MPa)	Relevant Elements
Bai et al. (1999)	IHPV: Quench	DCP-AES/AAS/ICP-MS	750 to 800	100 to 400	Na (0.03 - 4.01); K (0.01 - 2.41); Cu (0.5 - 98.9); Rb (0.006 - 1.63); Sr (0.002 - 2.98)
Borchert et al. (2009)	HDAC: Quench	SR-µXRF	750	200 to 700	Rb (0.01 - 0.47); Sr (0.0006 - 0.24)
Borchert et al. (2010)	CSPV/IHPV/HDAC: Quench	ICP-AES/IC/SR-µXRF	750 to 950	100 to 1400	Cl (2.01 - 119.28); Rb (0.002 - 0.81); Sr (0.001 - 0.57)
Bos (1990)	IHPV: Quench	ICP-OES	750 to 850	200 to 500	Na (0.41 - 1.63); K (0.18 - 1.08); Li (0.01 - 1.85); Cu (0 - 166); Zn (0 - 42.7); Rb (0.36 - 1.49)
Candela and Holland (1984)	CSPV: Quench	AAS	750	140	Cu (1.6 - 50)
Chevychelov and Chevychelova (1998)	CSPV/IHPV: Quench	EPMA	800 to 1000	100 to 500	Zn (1.2 - 7.1)
Holland (1972)	CSPV: Quench	AAS	850	200	Na (0.25 - 2.82); K (0.18 - 1.86); Ca (0.068 - 2.82); Cl (20 - 350); Mn (0.74 - 43); Zn (0.8 - 59)
Iveson et al. (2019)	IHPV: Quench	ICP-MS/Chloridometery	850 to 1050	60 to 200	K (0.11 - 1.56); Cl (3.06 - 37.4); Li (0.05 - 1.17); Mn (0.13 - 3.88); Cu (5.4 - 82.4); Zn (0.36 - 20.3);

					Rb (0.07 - 2.39); Sr (0.0005 - 0.81)
Keppler and Wyllie (1991)	CSPV: Quench/Mass Balance	DCP-AES	750	200	F (0.7 -1.1); Cu (1 - 83)
London et al. (1988)	CSPV: Mass Balance	Mass Balance	650 to 775	200	Na (0.1); K (0.1); F (0.3 - 0.4); Li (0.3 - 0.4); Be (0.2); Rb (0.1 - 0.2); Sr (0.4 - 0.5)
Schmidt et al. (2020)	CSPV: Synthetic Inclusions/Mass Balance	LA-ICP-MS	750	200	Na (0.76 - 0.91); K (0.47 - 0.81)
Simon et al. (2006)	CSPV: Synthetic Inclusions	LA-ICP-MS	800	140	Cu (27 - 102)
Tattitch et al. (2021)	CSPV/Piston Cylinder: Synthetic Inclusions	LA-ICP-MS	800 to 950	50 to 800	Cl (0.63 - 505)
Tattitch and Blundy (2017)	CSPV: Synthetic Inclusions	LA-ICP-MS	725 to 810	100 to 200	Cu (140 - 310)
Tattitch et al. (2015)	CSPV: Synthetic Inclusions	LA-ICP-MS	800	100	Cu (1.6 – 9.9)
Urabe (1987)	IHPV: Quench	AAS	800	100 to 500	Zn (0.05 to 23.04)
Webster et al. (1989)	IHPV: Mass Balance	Mass Balance	770 to 950	50 to 400	Li (0.2 - 12.6); Be (0.1 - 1.3); Rb (0.3 - 4.5); Sr (0.1 - 6)
Webster (1990)	CSPV/IHPV: Mass Balance	Mass Balance	775 to 1000	50 to 500	F (0.13 - 1.11)
Webster (1992)	CSPV/IHPV: Mass Balance	Mass Balance	800	200	Cl (17.3 - 117.5)
Williams et al. (1995)	CSPV: Quench	AAS	800 to 850	50 to 100	Cu (4 - 433)
Williams et al. (1997)	CSPV: Quench	AAS	800 to 850	50 to 100	Na (0.01 - 2.346); K (0.009 - 1.008)

Previous experiments reporting partition coefficients for the partitioning of metal between fluids and melts. The fluid "type" refers to the form in which the fluid was analyzed, i.e. as a quenched fluid that is recovered, as a fluid inclusion, or through a mass balance. The elements relevant to this study and the range of partition coefficients reported are also given.

Table 2:

Bishop Tuff		Fluids		
wt%	Starting Material	M	S4	S5
SiO_2	76.1(2)	NaCl	0.25	1
Al_2O_3	12.5(1)	KCl	0.25	1
TiO_2	0.061(3)	HCl	0.0001	0.0001
FeO	0.65(4)			
MnO	0.0321(3)			
MgO	0.08			
CaO	0.47(2)			
Na_2O	3.61(4)			
K_2O	5.11(4)			
Total	98.6(2)			

ppm	
Li	31.4(2)
Be	4.3(1)
Cu	5.42(5)
Zn	27.8(3)
Rb	174.5(7)
Sr	5.6(1)

Composition of staring Bishop Tuff Glass and aqueous chloride solutions. The composition of the Bishop Tuff is given in wt%. The compositions of the aqueous chloride solutions are given in molar (M). Uncertainty in the last digit(s) reported is given in parentheticals.

Table 3:

Run	Starting Glass (g)	Starting Fluid (g)	Starting Quartz (g)	Melt[a] (g)	Supercritical Fluid[a] (g)	Quench Type	Temperature (°C)	Pressure (MPa)	Duration (hours)	f_{O_2} (ΔQFM)
BT-1-S4	0.0254	0.0254	0.0294	0.027	0.026	Slow	800	192	142.75	-0.335(4)
BT-1-S5	0.0246	0.0272	0.0269	0.025	0.027	Slow	800	192	142.75	-0.335(4)
BT-2-S4	0.0489	0.0239	0.0260	0.049	0.023	Slow	800	198	141.75	-0.38(1)
BT-2-S5	0.0524	0.0267	0.0353	0.052	0.026	Slow	800	198	141.75	-0.38(1)
BT-4-2-S4[b]	0.0245	0.0258	0.0306	0.044	0.025	Slow	800	192	263	-0.42(1)
BT-7-S4	0.0514	0.0506	0.0287	0.0553	0.0493	Drop	800	196	163 +1	-0.09(1)

[a]Melt and Supercritical Fluid refer to the mass of the melt and supercritical fluid phase present during the experiment at 800°C and 200 MPa. [b]0.0014 grams of NaF:KF:AlF_3 mixture and 0.0015 grams of amorphous SiO_2 was added. Runs BT-1-S4/S5 and BT-2-S4/S5 were completed by loading the capsules into the vessel at the same time. S4/S5 correspond to fluid composition given in Table 2. The duration of experiment BT-7-S4 include one additional hour before drop quench. The digit in parenthetical is the uncertainty in the last digit in measured oxygen fugacity by CoPd sensors.

Table 4:

Glass						
wt%	BT-1-S4	BT-1-S5	BT-2-S4	BT-2-S5	BT-4-2-S4	BT-7-S4
SiO_2	72.1(1)	72.4(1)	71.8(2)	73.0(3)	71.0(2)	72.3(1)
Al_2O_3	11.00(9)	10.9(1)	10.85(7)	10.6(2)	10.88(8)	11.49(8)
TiO_2	0.0599(2)	0.0627(3)	0.0621(5)	0.0635(2)	0.0548(5)	0.06(1)
FeO	0.49(5)	0.39(4)	0.47(2)	0.5(1)	0.49(2)	0.39(4)
MnO	0.0212(1)	0.0061(1)	0.0243(2)	0.0094(2)	0.0216(2)	0.019(4)
MgO	0.08	0.07	0.07	0.08	-	0.08
CaO	0.42(1)	0.30(1)	0.41(1)	0.34(2)	0.11(1)	0.38(1)
Na_2O	3.12(2)	3.08(3)	3.15(4)	3.09(5)	3.29(5)	3.24(3)
K_2O	4.89(7)	5.25(6)	4.62(8)	5.02(7)	4.99(4)	4.92(1)
P_2O_5		0.11		0.09	0.09	
F					0.94(2)	
Cl	0.066(3)	0.128(7)	0.073(4)	0.151(7)	0.071(3)	0.090(6)
Total	92.2(2)	92.7(2)	91.5(2)	93.0(4)	91.9(2)	93.0(2)
-O = F,Cl	0.01	0.03	0.02	0.03	0.41	0.02
Total	92.2(2)	92.7(2)	91.5(2)	92.9(4)	91.5(2)	93.0(2)
H_2O	5.7(4)	5.3(3)	6.3(4)	5.1(3)	6.0(4)	5.0(3)
Total with H_2O	97.9(4)	98.0(4)	97.8(5)	98.0(5)	97.5(5)	98.0(4)
ppm						
Li	26.9(1)	18.1(1)	30.7(2)	24.77(9)	21.7(4)	28.24(1)
Be	3.98(2)	4.01(4)	4.00(8)	4.03(6)	3.14(6)	3.95(1)
Cu	0.41(2)	0.41(2)	0.38(1)	0.393(5)	0.42(1)	0.36(7)
Zn	6.5(1)	5.1(1)	3.64(5)	4.8(1)	19.1(9)	8.88(1)
Rb	146.2(5)	105.7(3)	162.6(9)	135.4(2)	141.3(6)	142.354(3)
Sr	5.32(3)	4.25(2)	5.43(6)	4.99(4)	4.2(2)	4.85(1)
Fluid						
mg/L or ppm	BT-1-S4	BT-1-S5	BT-2-S4	BT-2-S5	BT-4-2-S4	BT-7-S4
Na^+	6600(500)	18000(2000)	5900(500)	20000(2000)	5400(400)	4100(500)
K^+	6100(200)	24000(2000)	5600(200)	21400(900)	4600(200)	5900(200)
Ca^{2+}	410(20)	1000(100)	310(10)	1030(40)	710(30)	-
F^-	570(20)	580(60)	-	-	640(20)	51(1)
Cl^-	13800(600)	65000(6000)	13600(500)	55000(2000)	5000(200)	17000(1000)

Li	5.6(6)	15(2)	5.7(6)	21(2)	4.2(4)	6.5(6)
Be	0.08(1)	0.08(1)	0.08(1)	0.08(1)	0.21(2)	0.02(2)
Mn	81(8)	180(20)	110(10)	340(30)	32(3)	100(10)
Cu	21(2)	26(3)	12(1)	45(4)	160(20)	23(2)
Zn	46(5)	84(8)	49(5)	130(10)	140(10)	49(5)
Rb	24(2)	64(6)	24(2)	86(9)	17(2)	24(2)
Sr	0.24(2)	1.2(1)	0.13(1)	1.3(1)	0.75(7)	0.14(1)

Composition of run product glasses and fluids. Glass compositions determined by EPMA and LA-ICP-MS and are reported in wt% or ppm, respectively. Elements analyzed by ion chromatography are indicated by a charge associated with that element and are reported in mg/L, all other elements are determined by solution ICP-MS and reported in ppm. Uncertainty in the last digit(s) reported is given in paratheatrical. Uncertainty for EPMA and LA-ICP-MS of the run product glass is the standard deviation of the mean (σ_m), determined by the equation: $\sigma_m = \left(\sqrt{\frac{1}{n-1}\sum_{i=1}^{n}(x-\bar{x})^2}\right)/\sqrt{n}$ where n is the number of measurements. For major elements measured by EPMA in glass n = 10. For trace elements measured by LA-ICP-MS in glass n = 5. All analytical points were chosen at random across the glass shards. Uncertainty for ion chromatography analyses is estimated from the reproducibility of the standards. Uncertainty for solution ICP-MS is estimated to be ~10%. Uncertainties for ion chromatography and ICP-MS measurements for solutions are better than 10% for all listed elements and are estimated by repeated analyses of in-house standards and certified reference materials (see text for additional details).

Table 5:

mg/L or ppm	BT-1-S4	BT-1-S5	BT-2-S4	BT-2-S5	BT-4-2-S4	BT-7-S4
Na	7900(500)	25300(500)	12700(800)	30700(800)	10400(600)	6700(400)
K	9100(700)	35700(700)	18000(1000)	40400(900)	13000(800)	8300(500)
Ca	140(90)	1080(80)	700(200)	1800(200)	3900(100)	400(100)
F	0	0	0	0	-400(-2300)	0
Cl	16300(100)	64200(300)	16400(100)	65600(400)	16500(100)	16740(50)
Li	3.0(5)	11.9(4)	7.1)	13.4(9)	11.7(7)	1.0(5)
Be	0.1(1)	0.3(1)	0.0(2)	0.6(2)	1.4(2)	0.1(1)
Mn	74(3)	180(3)	124(6)	359(5)	102(4)	98(3)
Cu	4.91(6)	4.50( )	10.8(1)	10.3(1)	7.81(9)	5.27(6)
Zn	20.7(4)	20.3 3)	51.8(7)	47.1(7)	11(1)	19.1(4)
Rb	20(1)	6 (1)	22(2)	80(2)	30(2)	22(1)
Sr	0.0(-1)	1.2(1)	0.2(2)	1.2(2)	1.6(2)	0.4(1)

Concentrations of run product fluid calculated by mass balance. Uncertainty in the last digit(s) is given in parentheticals. The uncertainty in the mass balance calculation is calculated by propagating the uncertainty in EPMA analyses of the glass run product reported in Table 4 and the uncertainty in weighing. The uncertainty on the analytical balance is 0.1 mg. This uncertainty likely represents a minimum uncertainty. Negative concentrations for the mass balance calculations are a physical impossibility but are reported to show the degree to which the mass balance calculations are incorrectly calculated the concentration of some elements.

Table 6:

Measured					
BT-1-S4	BT-1-S5	BT-2-S4	BT-2-S5	BT-4-2-S4	BT-7-S4
Na 0.29(2)	0.79(8)	0.25(2)	0.89(7)	0.22(2)	0.17(2)
K 0.15(1)	0.54(5)	0.15(1)	0.51(2)	0.111(4)	0.145(4)
Ca 0.14(1)	0.45(5)	0.105(5)	0.42(3)	0.91(6)	-
F -	-	-	-	0.068(3)	-
Cl 21(1)	50(6)	18(1)	36(2)	7.1(4)	19(2)
Li 0.21(2)	0.83(8)	0.19(2)	0.85(9)	0.19(2)	0.23(2)
Be 0.019(2)	0.019(2)	0.021(2)	0.021(2)	0.065(7)	0.005(1)
Mn 0.49(5)	3.8(4)	0.56(6)	4.6(5)	0.19(2)	0.7(2)
Cu 52(6)	65(7)	32(3)	110(10)	380(40)	60(10)
Zn 7(1)	16(2)	14(1)	28(3)	7(1)	5(1)
Rb 0.16(2)	0.61(6)	0.14(1)	0.63(6)	0.12(1)	0.17(2)
Sr 0.045(5)	0.28(3)	0.023(2)	0.26(3)	0.18(2)	0.029(3)

Mass Balance					
BT-1-S4	BT-1-S5	BT-2-S4	BT-2-S5	BT-4-S4-2	BT-7-S4
Na 0.34(2)	1.11(3)	0.54(4)	1.34(4)	0.43(3)	0.28(2)
K 0.22(2)	0.81(2)	0.47(3)	0.97(3)	0.31(2)	0.20(1)
Ca 0.05(3)	0.51(4)	0.25(7)	0.75(9)	5.0(3.1)	0.15(4)
F 0	0	0	0	-0.05(-0.24)	0
Cl 25(1)	50(3)	23(1)	43(2)	23(1)	19(1)
Li 0.11(2)	0.65(2)	0.02(4)	0.54(4)	0.54(3)	0.04(2)
Be 0.03(3)	0.07(2)	0.16(6)	0.15(5)	0.44(5)	0.02(3)
Mn 0.45(2)	3.78(7)	0.66(3)	4.92(14)	0.61(3)	0.69(16)
Cu 12.0(5)	11.0(5)	28.2(9)	26.2(5)	18.5(5)	15(3)
Zn 3.18(9)	4.0(1)	14.2(3)	9.9(3)	0.55(7)	2.15(5)
Rb 0.14(1)	0.58(1)	0.13(1)	0.59(2)	0.21(1)	0.16(1)
Sr -0.002(-0.02)	0.28(2)	0.04(4)	0.25(4)	0.38(4)	0.08(2)

Partition coefficients determined from measured compositions and mass balance calculations. Uncertainty in the last digit(s) is reported in parentheticals and is propagated from the uncertainty in analyses reported in Table 5. Negative partition coefficients for mass balance calculations are a physical impossibility put are reported for comparative purposes and to present the degree to which mass balance calculations are incorrect.

Figure 1: Step-by-step procedure for the recovery and analysis of run product fluids and glasses.

Figure 2: Variation in Na, K, Rb, and Cu as a function of chlorine in the fluid phase. Error bars the uncertainties reported in Table 4.

Figure 3: Line scans from drop and slow quench glasses with sodium/potassium ratios determined from standardless semi-quantitative EDS analyses. Each point represents one EDS spectra and each line scan includes 100 equally spaced points. Two line scans were taken for experiments BT-2-S4, BT-2-S5, and BT-7-S4. Parentheticals indicate the type of quench for each experiment.

Figure 4: Comparison of measured concentration of the fluid phase compared to the concentration computed by mass balance. Red line indicates a one-to-one relationship. Error bars the uncertainties reported in Table 4 and 5.

Figure 5: Sodium + potassium (*m*; molal) plotted against chlorine (*m*) for the mass balance and measured composition. The line indicates a one-to-one relationship.

Figure 6: Comparison of previously reported partition coefficients to partition coefficients reported in this study. The range of partition coefficients reported in the literature for synthetic fluid inclusions, quench fluids, and those calculated by mass balance are represented by rectangles. The open red circles are high HCl-bearing solutions and are outliers of the data from Bai et al. (1999). Closed red circles are partition coefficients of the present study derived from measured values. Closed blue circles are partition coefficients of the present study derived from mass balance calculations. All studies used to generate the rectangles are given in Table 1 along with the experimental methods and type of analyses used. The partition coefficients of Shinohara et al. (1989) for sodium and potassium have been excluded due to the ion exchange noted in that study (see text).

Highlights

- Complete recovery of quenched fluids from magmatic-hydrothermal experiments
- Direct analyses of fluids from high-pressure, high-temperature experiments
- Direct analyses are more accurate than mass balance calculations

Construction of Experimental Capsule and Experiment

• Capsule configuration for all experiments

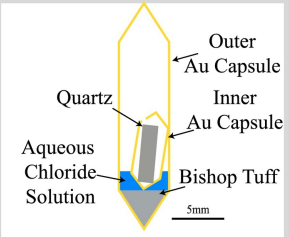

• Experimental Conditions:
  Pressure: 200 MPa
  Temperature: 800°C
  Duration: 6-11 days
  f_{O_2}: ~QFM
  Quench:Drop/"Slow"

Fluid and Glass Recovery

1. Capsule cleaned in acetone and weighed

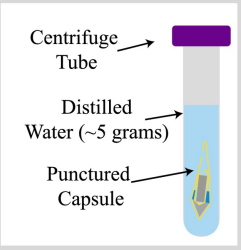

2. Place capsule in ~5 grams of distilled water inside a centrifuge tube, puncture capsule, and soak for a minimum of one week. (Soak solution)

3. After one week remove capsule and sample 5µl of the water, placing sample in glass vial.

4. Dry capsule at 120°C overnight

5. Weigh Capsule: Mass change is the mass of quenched fluid

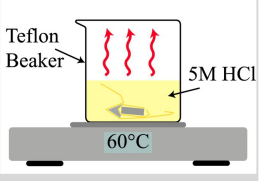

6. Open capsule with razor blade and re-weigh to account for any gold lost during opening

7. Place opened capsule in ~10 grams of 5M HCl inside a clean Teflon beaker at 60°C for 20 minutes (HCl solution)

  • Beakers are cleaned in 6M HCl for 24 hours at 120°C followed by 7M HNO_3 for 24 hours at 120°C

8. Remove capsule and dry at 120°C overnight

9. Weigh Capsule: Mass change is the mass of precipitates

10. Mass of liquid + mass of precipitates = mass of volatile phase

11. Mix soak solution and HCl solution

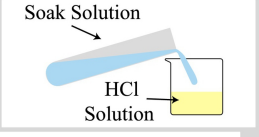

12. Heat mixed solution at 60°C until dry

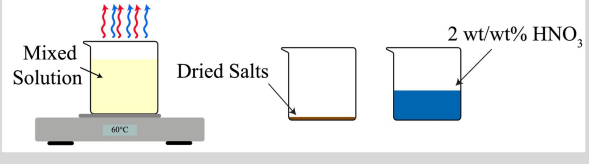

13. Re-dissolve salts in 5 grams of 2 wt/wt% HNO_3

14. Remove quartz and weigh to determine mass of melt by difference. Mount glass in epoxy.

Analyses

• Fluid:
  1. Soak solution from step 3 is analyzed by ion chromatography for Cl^-, F^-, Na^+, K^+, Ca^{2+}
  2. Nitric acid solution from step 13 analyzed by ICP-MS for trace elements

• Glass:
  1. Major elements measured by EPMA
  2. Trace elements measured by LA-ICP-MS

Figure 1

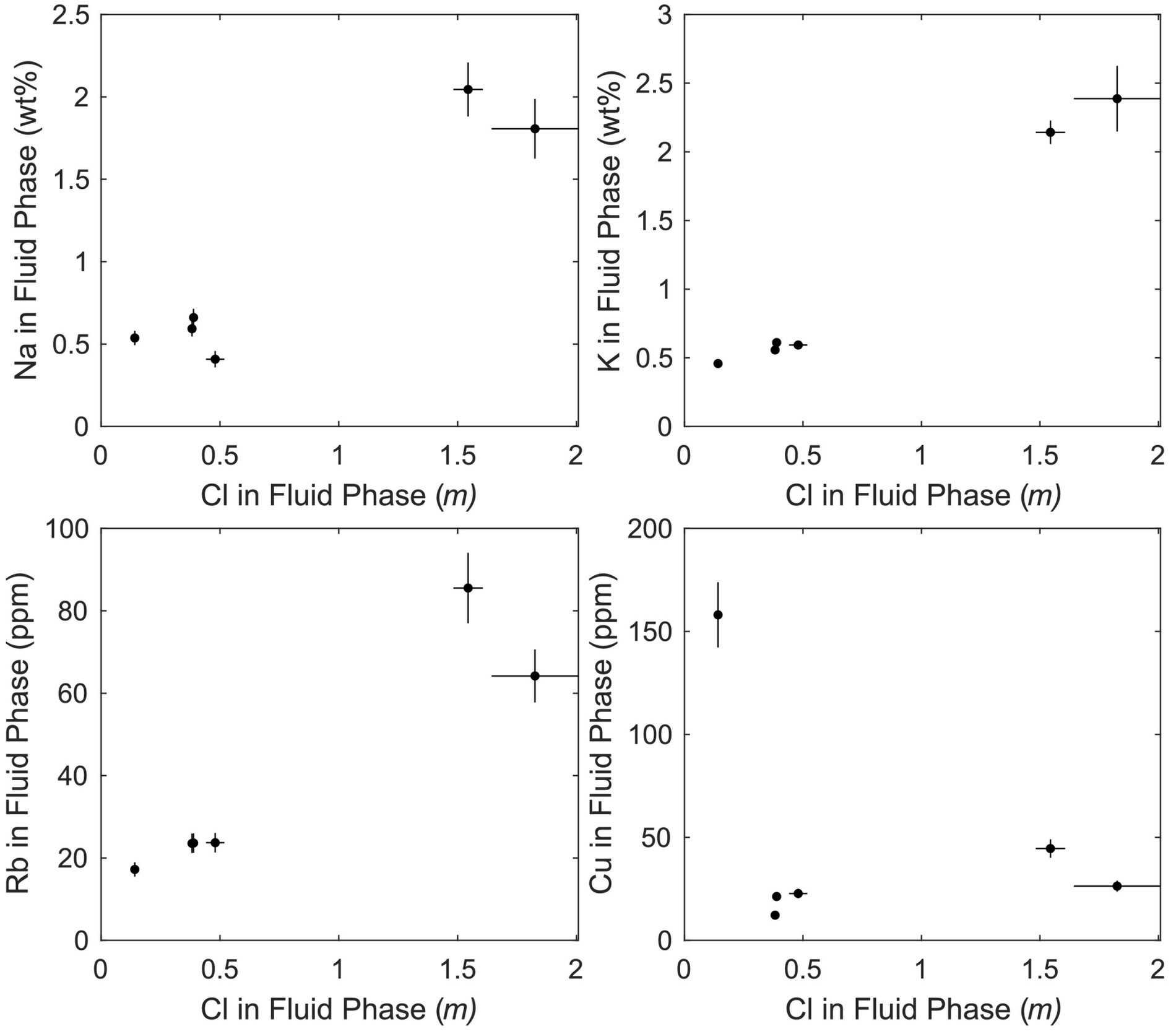
Na in Fluid Phase (wt%)
Cl in Fluid Phase (m)
K in Fluid Phase (wt%)
Cl in Fluid Phase (m)
Rb in Fluid Phase (ppm)
Cl in Fluid Phase (m)
Cu in Fluid Phase (ppm)
Cl in Fluid Phase (m)

Figure 2

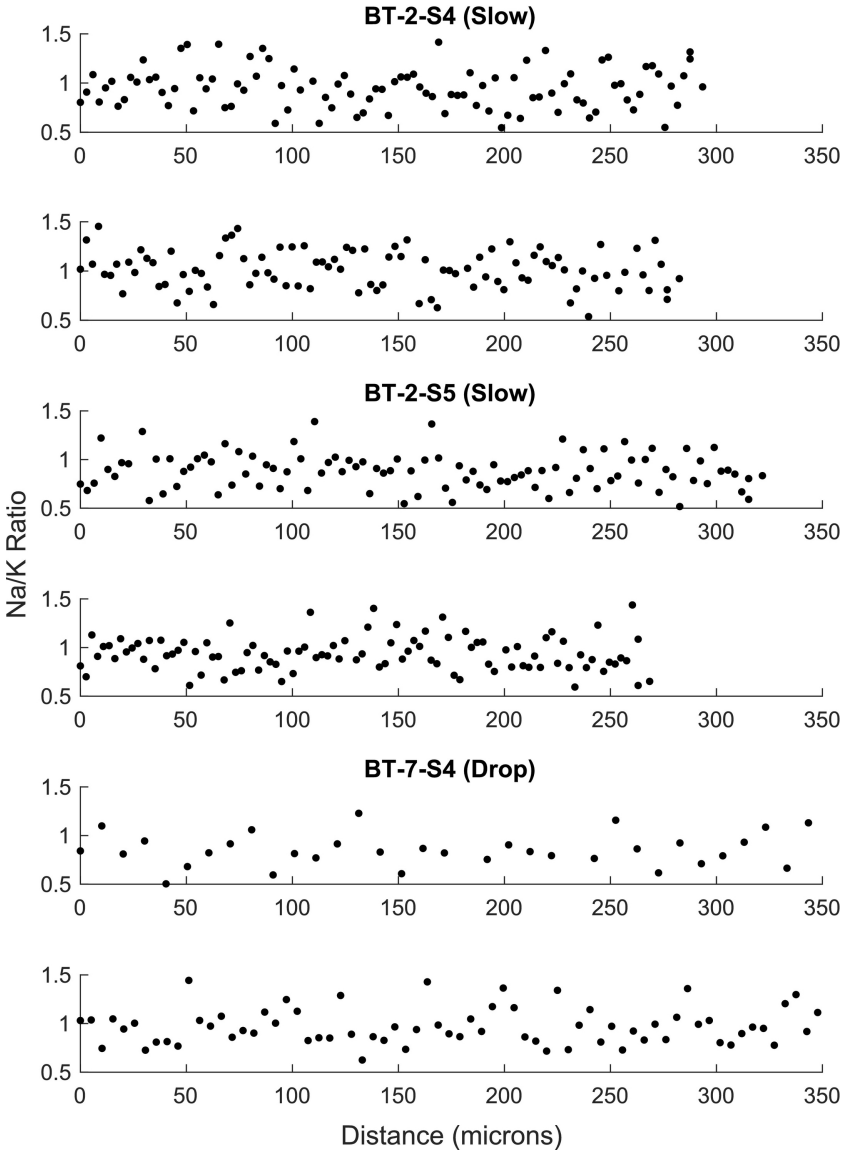
BT-2-S4 (Slow)
BT-2-S5 (Slow)
BT-7-S4 (Drop)
Na/K Ratio
Distance (microns)
1.5
1
0.5
0
50
100
150
200
250
300
350

Figure 3

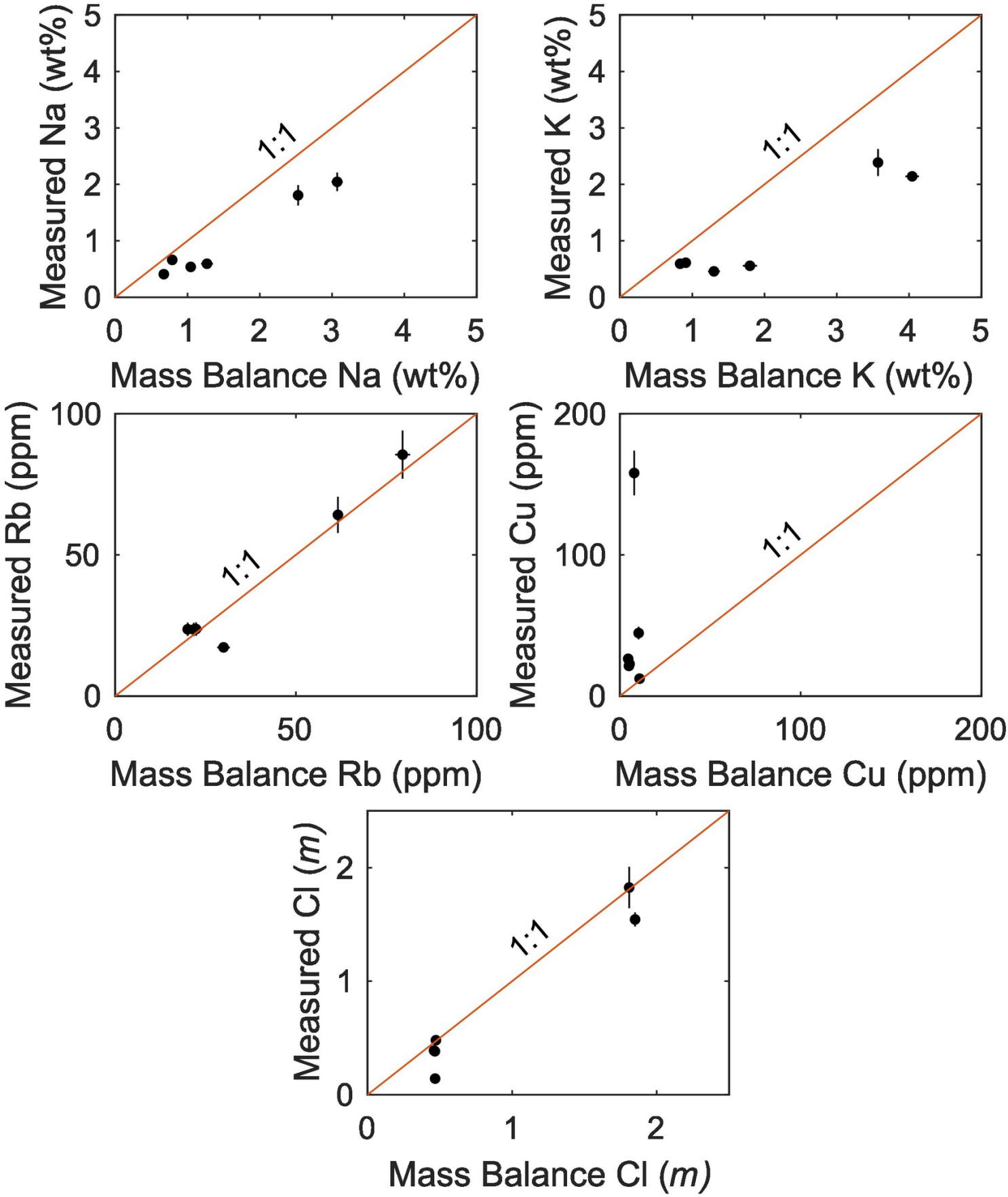
Measured Na (wt%)
Mass Balance Na (wt%)
1:1
Measured K (wt%)
Mass Balance K (wt%)
1:1
Measured Rb (ppm)
Mass Balance Rb (ppm)
1:1
Measured Cu (ppm)
Mass Balance Cu (ppm)
1:1
Measured Cl (m)
Mass Balance Cl (m)
1:1

Figure 4

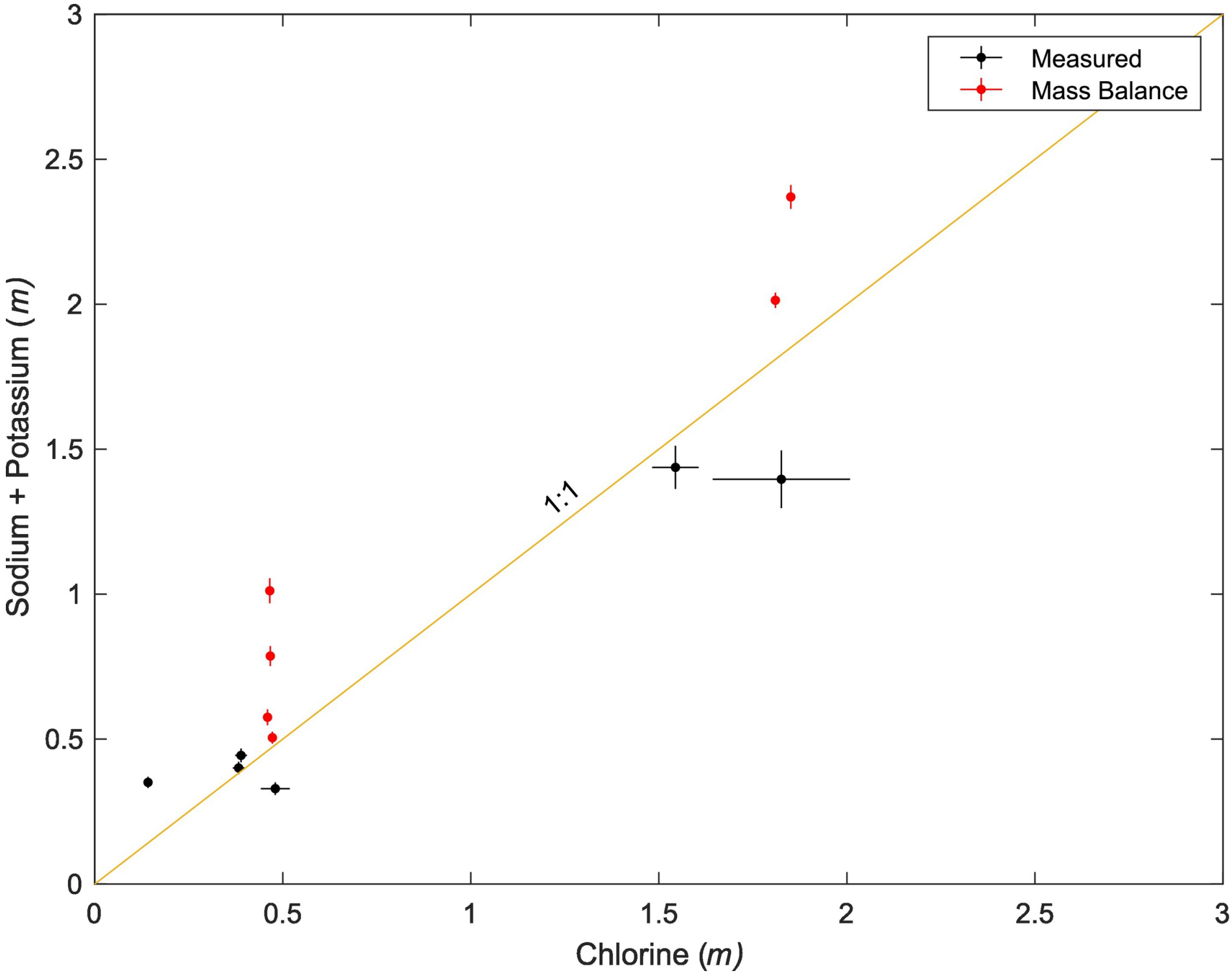
Measured
Mass Balance
1:1
Sodium + Potassium (m)
Chlorine (m)
0
0.5
1
1.5
2
2.5
3

Figure 5

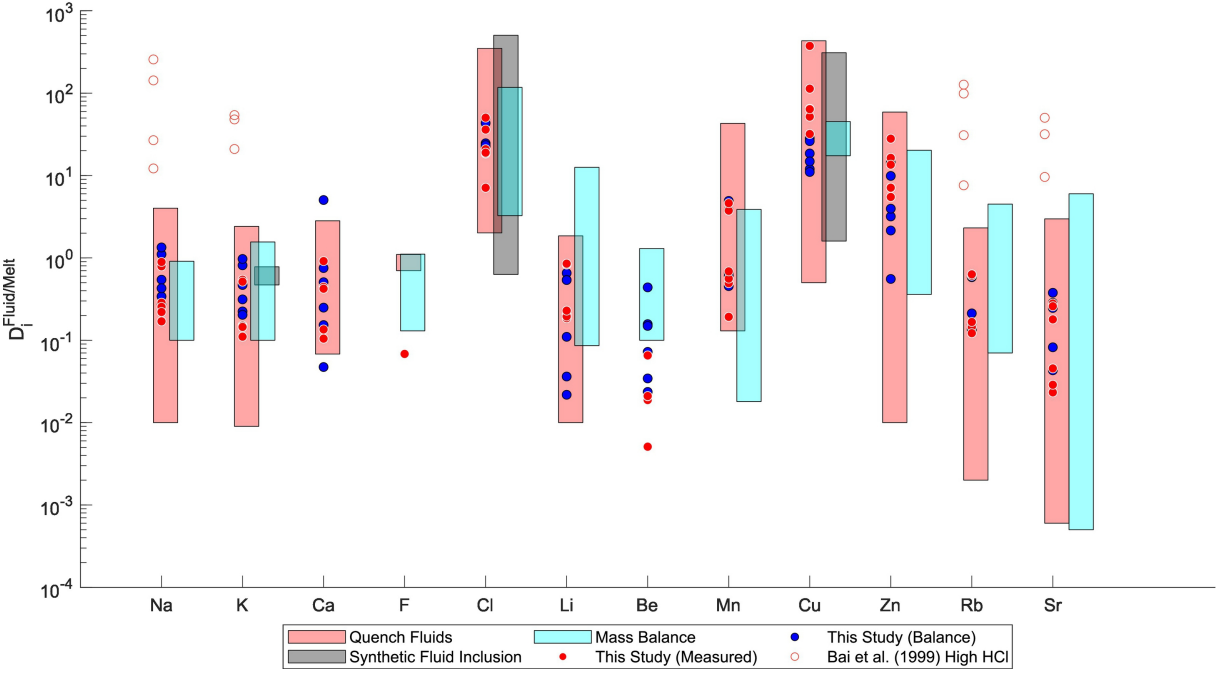
$D_i^{Fluid/Melt}$
10^3
10^2
10^1
10^0
10^{-1}
10^{-2}
10^{-3}
10^{-4}
Na
K
Ca
F
Cl
Li
Be
Mn
Cu
Zn
Rb
Sr
Quench Fluids
Synthetic Fluid Inclusion
Mass Balance
This Study (Measured)
This Study (Balance)
Bai et al. (1999) High HCl

Figure 6